Miner Deposita (2018) 53:547–564
DOI 10.1007/s00126-017-0754-4

ARTICLE

Geochemistry and mineralogy of Pd in the magnetitite layer within the upper gabbro of the Mesoarchean Nuasahi Massif (Orissa, India)

Hazel M. Prichard[1] · **Sisir K. Mondal**[2] · **Ria Mukherjee**[3] · **Peter C. Fisher**[1] · **Nicolas Giles**[1]

Received: 26 October 2016 / Accepted: 26 June 2017 / Published online: 20 July 2017

Abstract Palladium concentrations of 1–3 ppm with an average Pt/Pd ratio of 0.15 have been located for the first time in a magnetitite layer in the Nuasahi Massif in Orissa India. This layer occurs at a high stratigraphic level in the complex and is nearly 4-km long and 5–12-m thick. The sections of the Pd-rich zone identified to date extend over a distance of 1 km at the southern end of the layer. Several phases of mineralization are evident. The first, primary assemblage of platinum-group minerals (PGM) contains Pd-sulfides (vysotskite), Pd-Pb alloys (zvyagintsevite), and a Pd-In alloy, a mineral probably new to mineralogy. These PGM are confined to central magnetite grains in the magnetitites. The magnetite grains with exsolved fine laths of ilmenite at centers are referred to as central magnetite grains. These central magnetite grains are commonly surrounded by blebs of ilmenite and magnetite that contain the majority of the PGM. These are dominated by Pd-antimonides, variably altered to Pd-oxides, and other PGM including $PtAs_2$ (sperrylite), RuS_2 (laurite), and IrRhAsS (irarsite/hollingwothite). Many of these PGM also occur in the interstitial silicates, with rare occurrences in the central magnetite grains. We propose that the platinum-group elements (PGE) crystallized during a minor sulfide saturation event that occurred as the magnetitites crystallized. This event produced the minor Cu-sulfides in these magnetitites. Later introduction of antimony and arsenic, during the alteration event that produced the blebby ilmenite and magnetite, led to the more primary PGM being succeeded by the main PGM assemblage, dominated by Pd-antimonides. These are associated with secondary Cu minerals and sperrylite. Subsequent oxidation during weathering in the hot wet Indian climate produced the Pd-oxides. The Nuasahi Massif is a sill-like Archean layered ultramafic-mafic intrusion genetically linked to high-Mg siliceous basalt or boninites and is characterized by unusually thick layers of chromitite. PGE are concentrated in these chromitites and in the base metal sulfide-bearing breccias in the overlying gabbro. The Pd in the magnetitites described here indicates the presence of a third level where PGE are concentrated and a magma that crystallized to produce PGE concentrations at three stratigraphic levels in the massif. This indicates that similar thin sill-like intrusions, hosting unusually thick chromitites, may also have PGE concentrations at a number of stratigraphic levels.

Keywords Platinum-group elements · Palladium · Magnetitite · Chromitite · Sill-like layered igneous complex · Upper gabbro unit · Nuasahi Massif

Editorial handling: M. Fiorentini

Hazel M. Prichard deceased

Electronic supplementary material The online version of this article (doi:10.1007/s00126-017-0754-4) contains supplementary material, which is available to authorized users.

✉ Sisir K. Mondal
sisir.mondal@gmail.com

[1] School of Earth and Ocean Sciences, Cardiff University, Cardiff CF10 3AT, UK

[2] Department of Geological Sciences, Jadavpur University, 188 Raja S.C. Mallik Road, Kolkata 700032, India

[3] School of Geosciences, University of the Witwatersrand, Johannesburg 2001, South Africa

Introduction

Magnetitite layers or magnetite-rich lithologies are a common occurrence in the upper parts of mafic and ultramafic igneous intrusions at a level where the magma is in the final stages of

fractional crystallization and is Fe- and Ti-enriched. There are several descriptions of platinum-group element occurrences in association with magnetitites in the upper parts of layered complexes worldwide. Some of the more well-known ones include the Bushveld Complex (Barnes et al. 2004) and the Stella Complex (Maier et al. 2003) both in the Republic of South Africa, the Rio Jacaré Sill in Bahia, Brazil (Sá et al. 2005), the Skaergaard Intrusion in Greenland (e.g., Nielsen et al. 2015), the Rincón del Tigre Complex in Bolivia (Prendergast 2000), the Birch Lake and Sonju Lake intrusions in the Duluth Complex in the USA (Hauck et al. 1997), and the Freetown Intrusion in Sierra Leone (Bowles et al. 2013).

Platinum-group element mineralization has been described previously from the Nuasahi Massif in Orissa India, which is famous for hosting PGE concentrations of up to 24 ppm in a base metal sulfide-bearing (BMS) breccia zone that contains clasts of chromitite (Mondal and Zhou 2010). It is located above the lower ultramafic unit at the base of the gabbro (Mondal and Baidya 1997; Mondal 2000; Mondal et al. 2001; Augé et al. 2002).

This paper describes PGE concentrations in the magnetitite layer that occurs in the upper part of the Nuasahi Massif. The data on the PGE in the magnetitite layer presented here forms part of a broader systematic study across the Nuasahi Massif undertaken to locate PGE concentrations throughout the stratigraphic units. This broader systematic study also showed that the chromitite layers in the ultramafic part of the complex are PGE-bearing, mainly Ru, Os, and Ir (Mondal and Prichard 2016). Our initial results indicated the presence of PGE in the magnetitite layer and this led to a more detailed examination of the distribution of the PGE throughout the magnetitite layer and a detailed investigation of the platinum-group minerals (PGM) to establish their paragenesis. A main aim of this paper is to describe this new occurrence of Pd in the magnetitite in the Nuasahi Massif, characterizing the mineralogy of the mineralisation and producing a model for the formation and subsequent modification of the PGM during the stages of alteration and weathering.

The Nuasahi Massif appears to belong to a particular group of thin, layered igneous complexes or sills that are characterized by unusually thick chromitite layers. Chromitites are found in large stratiform complexes such as the giant Bushveld Complex (e.g., Mondal and Mathez 2007; Naldrett et al. 2009) and the Stillwater Complex (Barnes et al. 2015) where chromitite layers are in the order of 1-m thick or less but extensive laterally. Chromitites also occur as discontinuous pods in ophiolite complexes such as in Kempirsai (e.g., Melcher et al. 1997). However, there is another group of chromitites that have thick chromitite layers stratigraphically 2–10-m thick including the Inyala and Railway Block of Zimbabwe (Stowe 1994; Prendergast 2008), the Ipueria-Medrado and Campo Formosa Complexes in Bahia (Lord et al. 2004), and the Bacuri Complex in Amapa, Brazil (Prichard et al. 2001). Sometimes, the chromitite layers are up to 100-m thick as in the Kemi Complex in Finland (Alapieti et al. 1989) and Black Thor in Ontario (Carson et al. 2013). These chromite-rich complexes are Archean complexes that have been called "conduit type" (Mukherjee et al. 2012; Mungall 2014; Lesher et al. 2014). Some of these complexes have sulfide-bearing breccias at the ultramafic and mafic gabbro contact and magnetitites at the upper part of the complex. The stratigraphy of these complexes is not always complete and so not all contain high-level magnetitites. Some of these complexes are PGE-bearing as for example in the chromitites in Campo Formosa and Bacuri. The ultramafic intrusions are in general relatively thin stratigraphically and considered to be served as conduits for komatiitic magmas at shallow crustal levels (Mungall 2014). The Nuasahi Massif in the Singhbhum Craton and similar Archean chromite deposits in India such as the Sukinda Massif (Singhbhum Craton) and Nuggihalli Complex (Western Dharwar Craton) are also "conduit" type sill-like layered ultramafic-mafic plutonic complexes originated from high-Mg siliceous basalt or boninite or low-Al komatiitic magmas (Mondal et al. 2006; Mukherjee et al. 2012).

The total distribution of PGE throughout the stratigraphy of these "conduit" type complexes is poorly documented. A second aim of this paper is to put this PGE occurrence in the magnetitites in context within the Nuasahi Massif and encourage study of PGE in other similar "conduit" type complexes.

Geology

The Nuasahi Massif

The Nuasahi Massif forms one of a number of chromitite-rich ultramafic-mafic sill-like layered complexes situated within early Archean metasediments and metavolcanics of the Iron Ore Group (IOG) greenstone belts in the Singhbhum Craton in Orissa state, located in the northeastern part of India (Fig. 1) (Mondal 2009; Mondal and Zhou 2010). In the Nuasahi-Nilgiri belt, metasediments and metavolcanics of the IOG are intruded by a sill-like ultramafic-mafic plutonic complex (Fig. 1B). The NNW-SSE trending Nuasahi Massif comprises a lower chromitite-bearing ultramafic unit and an upper intrusive unit of gabbro (Fig. 2). The lower ultramafic unit is an elongate body (~5 km × 0.4 km) which is thicker near the central and southern parts and narrow at the northern end. The ultramafic unit abuts IOG quartzite to the northern end of the plutonic complex, whereas the southern end is surrounded by laterite and latosoil. The upper gabbro unit has a U-Pb zircon age of 3.1 Ga and a Sm-Nd isochron age of 3.2 Ga (Augé et al. 2003). The ultramafic body has a dip of 60–80° towards the east and consists of enstatitite (>95% modal enstatite) at the base with a harzburgite unit, overlain

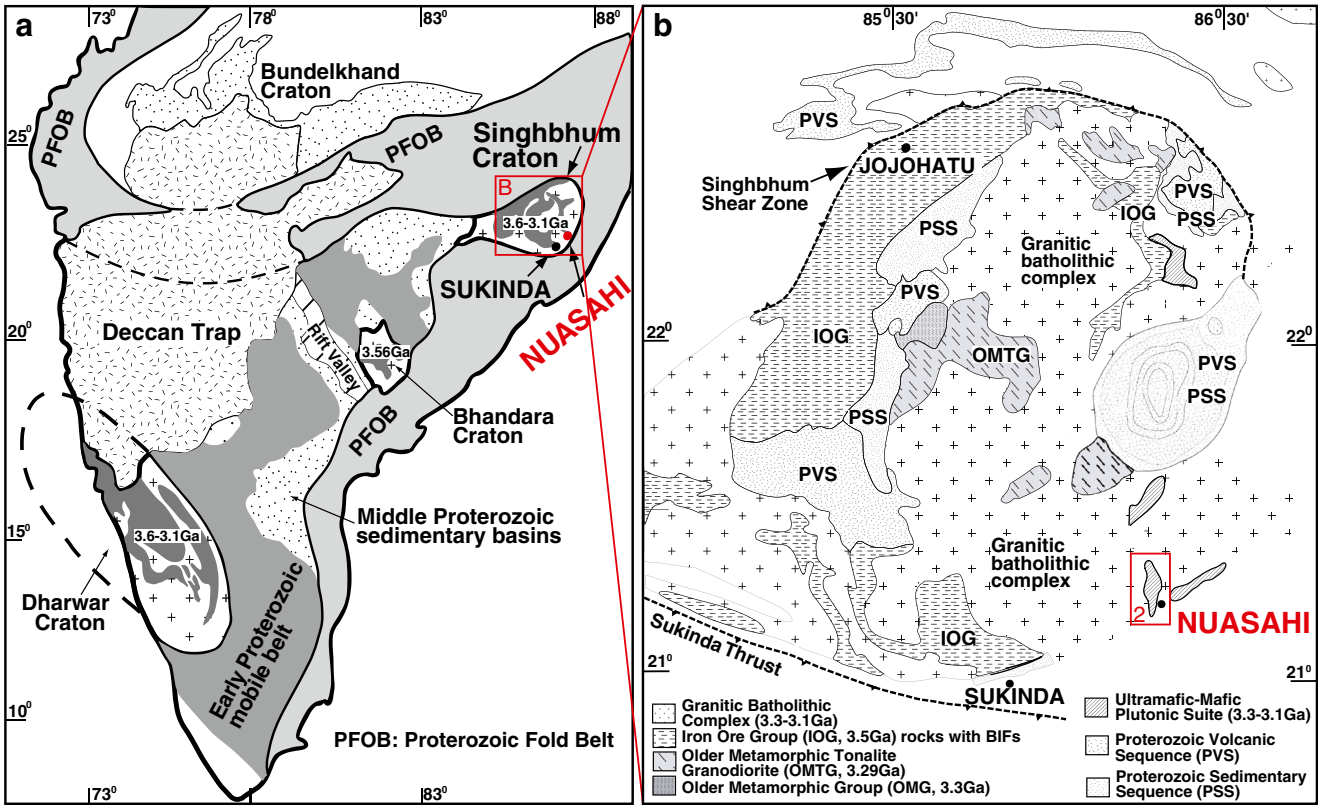

Fig. 1 Location and geology of the Nuasahi Massif. **a** Geological map of the Indian shield (compiled by Mondal et al. 2006 after Radhakrishna and Naqvi 1986; Leelananadam et al. 2006) showing the locations of the Singhbhum Craton and Nuasahi Massif. **b** Geological map of the Singhbhum Craton showing locations of the Nuasahi and Sukinda Massifs that contain chromite mineralization (compiled by Mondal et al. 2006 after Saha 1994; Sengupta et al. 1997)

by dunite (with a stratigraphic thickness of 130–150 m) and another orthopyroxenite unit (with a stratigraphic thickness of 80–120 m) (Mondal et al. 2006). Three chromitite ore bodies are hosted by the serpentinized dunite that are, from west to east, Durga (with a stratigraphic thickness of 3–4 m), Laxmi-2 (with a stratigraphic thickness of 2–3 m), and Laxmi-1 (with a stratigraphic thickness of 1.6–2 m) (Mondal et al. 2001, 2006). The chromitite layers are discontinuous but occur consistently throughout the belt and include massive, spotted, clot-textured, and schlieren-banded ores. The contact between the ultramafic and gabbro unit is marked by a 5-km-long × 10–15-m-thick breccia zone which thickens at the southern end (Mondal and Baidya 1997).

The overlying gabbro contains anorthosite layers and grades into diorite in the northeast. The gabbro textures and alteration are described in Khatun et al. (2014). Magnetite is a common phase in the gabbro and the modal concentration increases upwards. The gabbros occurring in the western, southern, and eastern part of the Nuasahi Massif are variably altered, shown by their mineral assemblage of quartz, amphibole, biotite, chlorite, muscovite, zoisite, sericite, epidote, ilmenite, leucoxene, sphene, and rutile. Sulfide disseminations (e.g., chalcopyrite, pyrite, violarite, bornite, and rare pyrrhotite) occur in the altered gabbro in the east. The gabbro is intrusive into the quartzite of the IOG supracrustal rocks belonging to the early Archean greenstone sequences in the west and also transgresses the ultramafic body where it intrudes the breccia zone in the east producing the matrix of the chromitite and ultramafic-clast supported breccia (Fig. 2). Small patches of the IOG rocks (quartzite and talc-chlorite-schist, chlorite-actinolite schist, and chlorite-tremolite schist) have been caught up and are present within the gabbroic rocks.

The magnetitite layer

At the top of the upper gabbro unit, to the east, there is a discontinuous layer of magnetitite (Ghosh and Prasada Rao 1952; Chakraborty 1959; Sarkar 1959; Varma 1964; Haldar and Chatterjee 1976; Chakraborty et al. 1988; Mondal 2000; Mohanty and Paul 2008; Mondal and Zhou 2010) which is the focus of this study. Varma (1964) reported at least four major separate discordant magnetitite bodies which are present within the gabbro-anorthositic host rocks. The largest one is ~2.4 km in length and ~12 m thick (trending E-W and dipping 57–60° N).

The discontinuous magnetitite bodies (total length ~4 km) are mainly located within the upper part of the gabbro (Fig. 2). The area is covered by tropical forest and outcrops are

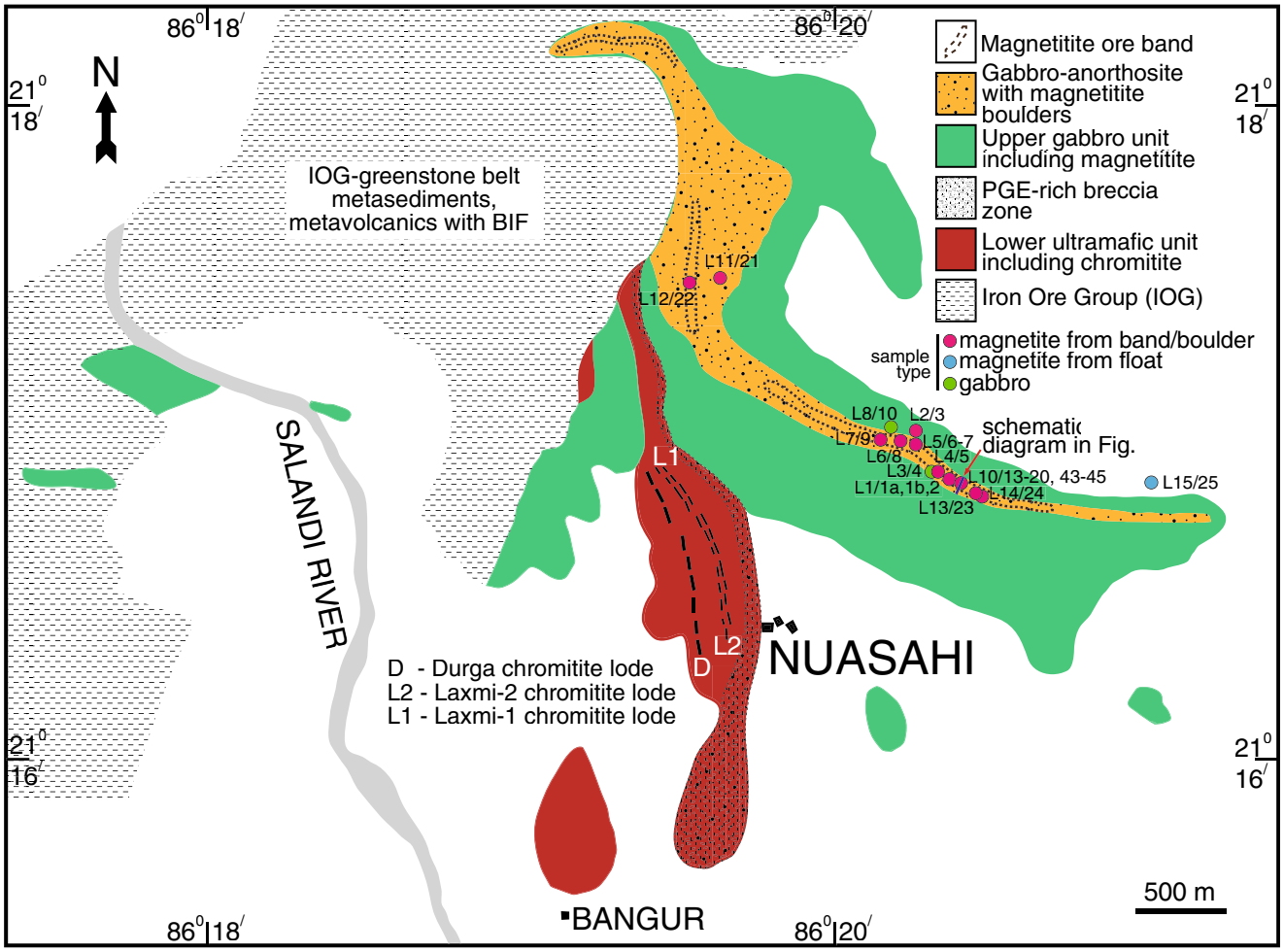

Fig. 2 Map of the Nuasahi Massif showing the chromitites, breccias, and magnetitite layer with locations. Map is modified from Ghosh and Prasada Rao (1952) and Mondal et al. (2006)

sporadic. Weathering of the host rocks results in the magnetitite standing out as ridges that are commonly 400- to 550-m long with thicknesses ranging between 5 to 12 m (Ghosh and Prasada Rao 1952). These magnetitite bodies can be joined up to form the whole magnetitite layer as the outcrop pattern of the bodies that are nearly concordant with the layering in the adjacent gabbro-anorthosite. The thickness therefore represents a stratigraphic thickness and the magnetitites have sharp contacts with their host gabbro. The strike of the layer varies from E-W in the north to N-S in the center and WNW-ESE in the south (Fig. 2) with a steep dip varying from 70° to the north and west to vertical.

The mineralogy and petrology of these magnetitites have been described previously (Chakraborty 1959). Varma (1986) reported intergrowths of ulvöspinel-magnetite, ilmenite-magnetite and hematite-magnetite, and rutile and hematite and martite replacing magnetite and rutile replacing ilmenite. Mohanty and Paul (2008) described the magnetitite as a closely packed mosaic of polygonal titanomagnetite grains (70 modal%) with variable amounts of ilmenite, hematite, and rutile. They observed goethite and lepidocrocite as fracture fillings and colloform bands replacing magnetite. The magnetitites have 0.16–1.02 wt% V_2O_5 (Chakraborty et al. 1988; Mohanty and Paul 2008). Mohanty and Paul (2008) also showed that V_2O_3 in magnetite ranges from 0.02 to 0.88 wt%, whereas in the coexisting ilmenite, V_2O_3 is generally lower (<0.27 wt%).

Methods

Samples of magnetitites were collected during two field seasons. In the first season in November 2013, only three magnetitite samples were collected. These were close to each other, just 2 m apart, located in the magnetitite layer situated at the uppermost part of a traverse that sampled across the whole stratigraphy of the Nuasahi Massif (Fig. 2, location 10, samples NSH/13/43–45). Out of these three magnetitite samples, two were initially analyzed for Pt, Pd, and Au by Pb sulfide fire assay followed by ICP-MS analysis (Intertek Genalysis Laboratories in Perth in Western Australia). The analysis showed that anomalous Pd and Pt concentrations are present

in the magnetitites (Table 1). This result led us to conduct a second field season in November 2014 to sample systematically along the strike of the magnetitite layer and also sample in a traverse across the layer at the initial sampling site (Figs. 2 and 3). Twenty-one magnetitite and two gabbro samples were collected and analyzed for all six PGE (Pt, Pd, Rh, Ir, Ru, and Rh) and Au by Ni sulfide fire assay followed by ICP-MS analysis at Intertek Genalysis. The three magnetitites collected in the first field season were also analyzed for all six PGE and Au with this batch of samples. The analytical results are shown in Table 1. The location of the samples and details of the controls on the analyses are presented as Electronic Supplementary Materials (ESM: Tables A−D) which are available online. All samples were submitted to the Intertek Genalysis as chips where these were quarantined and dry-crushed for analytical work. The base metals along with S and As were analyzed by four acid digestion method followed by ICP-MS at Intertek Genalysis.

The mineralogy was studied at Cardiff University using conventional optical microscopy, and minerals were analyzed using a Cambridge Instruments (now Carl Zeiss NTS) S360 scanning electron microscope (SEM). Polished blocks were searched systematically and manually for PGM using the four-quadrant backscattered electron detector (4QBSD) on the SEM set at a magnification of ×100, a magnification that allows PGM of 1–2 μm in diameter to be located. Quantitative

Table 1 PGE, Au, base metals, S and As analyses of magnetitite samples, and the host gabbro arranged from locality 11 in the north to locality 15 in the south (Fig. 2)

Sample no.	Au ppb	Ir ppb	Os ppb	Pd ppb	Pt ppb	Rh ppb	Ru ppb	Ag ppm	As ppm	Bi ppm	Co ppm	Cu ppm	Ni ppm	Pb ppm	S wt.%	Sb ppm	Sn ppm	Te ppm	Zn ppm	Pt/Pd
NSH/14/21	21	nd	nd	76	41	2	2													0.54
NSH/14/22	41	nd	nd	155	96	5	3	0.2	11	0.1	182	342	491	3.0	nd	4.9	2.0	nd	502	0.62
NSH/14/9	13	2	2	168	59	6	12													0.35
NSH/14/10[c]	8	nd	nd	25	2	2	2													0.08
NSH/14/8	11	nd	1	169	10	6	5													0.06
NSH/14/3	25	2	2	2487	61	13	36	0.1	2.1	0.2	186	826	380	3.4	nd	5.3	0.5	0.4	235	0.02
NSH/14/6	18	nd	2	121	11	6	5													0.09
NSH/14/7	22	nd	3	204	10	5	12													0.05
NSH/14/4[b]	7	nd	nd	433	21	3	7													0.05
NSH/14/5	27	2	2	1998	120	14	26													0.06
NSH/14/2	33	2	2	3078	84	17	48	0.1	2.1	0.1	188	292	918	6.8	nd	4.9	1.3	nd	492	0.03
NSH/14/1(a)	7	nd	nd	3	2	nd	nd													0.67
NSH/14/1(b)	21	1	2	765	51	7	16													0.07
NSH/14/20	358	nd	nd	1822	58	5	7													0.03
NSH/13/43[a]	42			3848	240															
NSH/13/43	44	4	3	3320	235	21	36	0.2	4.2	0.2	214	238	761	52	nd	6.3	1.1	0.3	415	0.07
NSH/13/45[a]	26			2380	110															
NSH/13/45	27	2	4	2219	107	12	27	0.7	5.1	0.1	218	703	606	14	nd	11	0.7	nd	426	0.05
NSH/13/44	25	3	3	1380	61	9	35													0.04
NSH/14/19	17	1	2	1294	44	7	21													0.03
NSH/14/18	20	2	2	1532	54	8	23													0.04
NSH/14/17	41	1	1	1138	90	7	13													0.08
NSH/14/16	22	2	2	1729	144	12	17													0.08
NSH/14/14	27	2	3	1411	86	11	21	0.1	4.8	0.1	241	234	461	3.5	nd	6.6	1.0	nd	527	0.06
NSH/14/13	25	nd	1	456	36	3	4													0.08
NSH/14/23	16	2	1	923	128	12	18	nd	6.0	0.2	205	136	569	5.1	nd	2.1	0.4	nd	391	0.14
NSH/14/24	38	2	2	1042	170	13	12	0.1	15	0.1	210	178	373	2.6	nd	9.1	0.8	nd	574	0.16
NSH/14/25	34	1	1	985	147	11	10													0.15

nd not detected

[a] Pb sulfide fire assay and ICP-MS; other samples were analyzed by Ni sulfide fire assay followed by ICP-MS for Au and platinum-group element and four acid digestion followed by ICP-MS for base metals, S and As

[b] Footwall gabbro

[c] Hanging wall gabbro

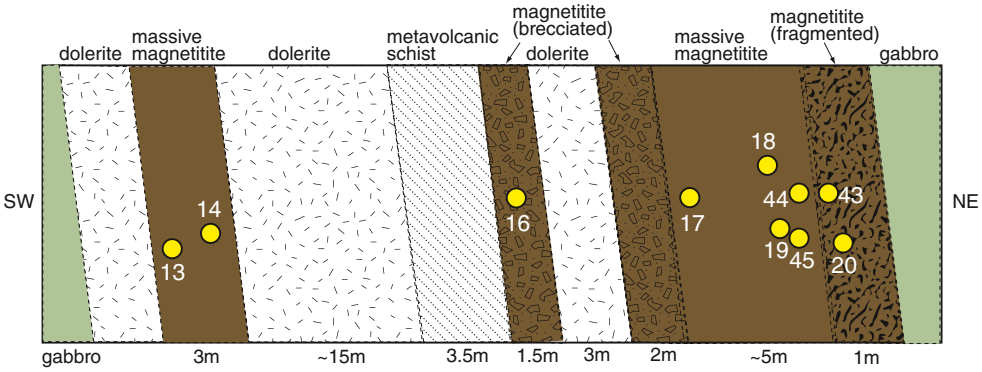

Fig. 3 Schematic diagram of the magnetitite layer at location 10 showing the different types of magnetitite and the locations of samples. Here the magnetitite body strikes 305–125° with a high angle (70–80°) dip to the east northeast

analyses of the larger PGM were obtained using an Oxford Instruments INCA Energy EDX analyzer attached to the SEM. Operating conditions for the quantitative analyses were 20 kV, with a specimen current of ~1 nA and a working distance of 25 mm. A pure cobalt reference standard was analyzed every five analyses in order to check for any drift in the analytical conditions. A comprehensive set of standards including Fe, Co, Rh, Ru, Os, Ir, Pt, and Sb all 99.99% pure or better, S in FeS_2, and As in InAs were used to calibrate the EDX analyzer. The standards were sourced from MicroAnalysis Consultants Ltd. (St Ives, Cambridgeshire). Images were photographed using a four-quadrant backscattered detector operating at 20 kV, a beam current of ~500 pA, and a working distance of 13 mm. Many PGM were either too small or too inhomogeneous for quantitative analysis and were analyzed qualitatively. To place the PGM in context mineralogically, the associated silicate and oxide minerals were analyzed qualitatively using the SEM. The size of each PGM in the polished sections was measured from SEM images in two directions at right angles in order to gain their area which was measured by multiplying the two values. The area represented is not an absolute value as the estimation does not consider the shape and size of the PGM in three dimensions. The PGM mineral analyses are summarized in Table 2.

Results

Magnetitite samples

The magnetitite samples vary from massive to friable where they are more weathered, and magnetitite outcrops are sometimes coated with a surface staining of malachite (ESM: Table A and Table 3). Sampling was focused in the more accessible parts of the magnetitite layer especially in the southern parts that have an ENE-WSW trend (Fig. 2). At four locations, no outcrop was visible and boulders were sampled that appeared not to have traveled far and were very likely to be derived from the underlying magnetitite. At location 10, where the original magnetitite samples were taken, it was possible to observe in greater detail the variation across the layer (Fig. 3). Here, the magnetitite is split into several layers and is intruded by a doleritic dyke. In the center of the layer, the magnetitite is brecciated with smaller sized fragments and at the top the magnetitite is fragmented with larger boulders. These boulders are occasionally altered with malachite staining. The rocks on the both sides of the magnetitite layer are bleached and appear to be anorthositic which is highly altered and weathered.

Mineralogy and geochemistry of the magnetitites

The magnetitite is usually very massive and formed of grains of magnetite that are adjacent to each other and are surrounded by interstitial altered silicates (Fig. 4a). These silicates include abundant chlorite that also occurs in veins and micro-veins that crosscut the magnetite grains. The centers of the magnetite grains have a very marked and consistently developed trellis texture of exsolved fine laths of ilmenite that occur along well-defined crystallographic planes (Fig. 4b). From here on in the text, these centers of magnetite grains with exsolved fine laths of ilmenite are referred to as central magnetite grains. Commonly, these central magnetite grains are surrounded by a mosaic of adjacent ilmenite and magnetite blebs (Fig. 4c). The texture of ilmenite lamellae in magnetite is quite common in the magnetitite samples. Ilmenite does not normally exsolve from magnetite. Usually, ulvöspinel exsolves along the (100) planes of the magnetite (there is magnetite-ulvöspinel solid solution). The ulvöspinel subsequently oxidizes to ilmenite (the oxy-exsolution of Buddington and Lindsley 1964).

These magnetite and ilmenite blebs are frequently in contact with interstitial silicates (Fig. 4d). In some cases, these blebs form more extensive areas than the central magnetite grains (Fig. 4e) and they occur with magnetite grains exhibiting more alteration and concentric growth patterns (Fig. 4f).

The central magnetite grains frequently contain 1–5 wt% Cr_2O_3. Central magnetite grains that contain lower amounts of Cr_2O_3 (1–2 wt%) may also contain ~0.5 wt% V_2O_5. The blebs

Table 2 Quantitative ED scanning electron microscope analyses of PGM

	Pd_7Sb_3	PdSb	Pd-Sb-O	Pd-Sb-O	Pd-Cu-O	$PtAs_2$	Pd_3Pb	CoFeAs	Pd_2S
wt%									
Pt						57.8			
Pd	67.7	45.8	51.0	60.7	64.6		62.0		86.7
Rh								2.8	
Pb							37.8		
Cu					10.7				
Ni								2.0	
Co								17.7	
Fe			15.2	7.4				19.6	
As						42.3		34.3	
Sb	30.8	54.1	21.6	26.0					
S								12.7	12.8
O			11.9	7.6	20.1			11.6	
Total	98.5	99.9	99.7	101.7	95.4	100.1	99.8	100.7	99.5
Atomic %									
Pt						34.5			
Pd	71.6	49.2	10.6	41.0	29.0		76.2		67.0
Rh								1.2	
Pb							23.9		
Cu					8.1				
Ni								1.5	
Co								13.1	
Fe			16.3	9.5				15.3	
As						65.6		20.0	
Sb	28.4	50.8	10.6	15.4					
S								17.2	33.0
O			44.5	34.2	59.9			31.7	

CoFeAs contains significant S and O and the Pd-Sb-O contains significant Fe

of magnetite and ilmenite on the edges of the grains typically do not contain Cr, but they are accompanied by rare Al-Fe-rich spinels containing ~6 wt% Cr_2O_3 (Fig. 4g). Copper sulfide minerals are sparse in these magnetitites but where they do occur they form chalcopyrite or are altered and include chalcocite (Fig. 4g) and covellite. Rare sulfarsenides belonging to the cobaltite-gersdorffite solid solution series are present in the blebby ilmenite and magnetite margin (Fig. 4h), and they are very Co-rich (25–30 wt% Co) and Ni-poor (0–3 wt% Ni). Rare zirconium oxides are present in the silicates.

PGE concentrations

Analyses for Pt and Pd in the two magnetitite samples collected (NSH/13/43 and NSH/13/45) as part of the initial sampling traverse across the stratigraphy of the Nuasahi Massif have values of 3848 and 2380 ppb Pd and 240 and 110 ppb Pt, respectively (Table 1). Subsequent analysis of 21 samples of magnetitites from locations along strike across the magnetitite layer confirmed the widespread occurrence of anomalous Pd concentrations and to a lesser extent anomalous Pt concentrations. Ten of the magnetitite samples have concentrations of over 1 ppm Pd and range up to 3 ppm (Table 1). Platinum values are consistently lower with the highest value of only 170 ppb. The average Pt/Pd ratio is 0.15 indicating that Pd is substantially enriched compared to Pt. Ruthenium is the next most abundant PGE with an average of 14 ppb and Rh has an average value of 8 ppb. Osmium and Ir are present at concentrations of 1–4 ppb in many of the magnetitite samples. Chondrite-normalized PGE patterns for the magnetitites have a positive slope rising steeply to Pd, with a slight rise at Ru (Fig. 5a) for the most enriched samples. A similar pattern is observed in the slightly less PGE-enriched samples (Fig. 5b).

The whole-rock PGE abundances in the magnetitite samples indicate that there is a nearly 1-km-long PGE zone along the strike of the magnetitite layer. This extends from location 14 to location 2 (Fig. 2 and Table 1). Except for sample NSH/14/1a, all the samples from this zone have a much higher PGE concentration (ΣPGE = 500–3619 ppb) than the samples from the northern continuation of the layer (ΣPGE = 49–269 ppb).

Table 3 Numbers of the different PGM in the magnetitite samples

	Sample	Pd-Sb	Pd-Sb-O	Pd-Cu-O	Pd-Pb	Pd-Te	$PtAs_2$	Au	RuS_2	RhIrAsS	CoAsS (Rh,Ru)	Pd-As	Pd-S	Pt-Fe	Pt-Pd	Pd-In	Pt	Pd	Sample description
Location 2	14/3	2	12				4	1			1						61	2487	Friable Mal B
Location 4	14/5	3															120	1998	Massive B
Location 1																			
Top	14/2	1	9														84	3078	Massive
Bottom	14/1B	7				1			1								51	765	Less massive Mal
Locality 10																			
Top	14/20	26					1	1							2		58	1822	Fragmented
	13/43	6		2	3		1										235	3320	Fragmented Mal
	13/45	19	28				4	1	1	2	1						107	2219	Weathered Mal
	13/44	2	2					3									61	1380	Massive
	14/19	9	1	1			4		2	1			1				44	1294	Massive
	14/18	3		15			4										54	1532	Massive
	14/17	4					1							1			90	1138	Massive
	14/16	10		3							1						144	1729	Brecciated
	14/14	12	1							1		2					86	1411	Massive
Bottom	14/13	3	3			1	2	2									36	456	Massive
Location 13	14/23	1		4	9		1		2			1	9		2	13	128	923	Massive coarse
Location 14	14/24	31	1				5										170	1042	Massive sheared
Location 15	14/25	2		1											1		147	985	Friable

Samples are arranged in geographic order from west to east (Fig. 2). *Top* indicates sampling has been conducted from the upper part of the magnetitite layer. *Bottom* indicates sampling has been conducted from the lower part of the magnetitite layer

Mal malachite staining on the surface of the magnetitite sample, *B* boulder

The sample from location 15 has a high PGE concentration (ΣPGE = 1155 ppb, Pd = 985 ppb) similar to the samples from the magnetitites to the west. This sample may indicate a continuation of the PGE zone in the magnetitite layer to the southeast. The whole-rock analyses also show that PGE distribution varies across the thickness of the magnetitite layer. For example, at both locations 1 and 10, samples from the upper part of the magnetitite layer have a higher PGE content than those from the stratigraphically lower part of the layer (Fig. 2 and Table 1). The whole-rock analyses also confirm the sulfide- and base metal-poor character of the PGE mineralization in the Nuasahi magnetitites (Ni = 373–918 ppm, Cu = 178–826 ppm, Co = 182–241 ppm, Zn = 235–574 ppm with negligible Ag and Pb values; Table 1). The S concentrations for this set of samples are below the detection limit with detectable As values (As = 2.1–15 ppm; Table 1).

Platinum-group minerals

More than 300 PGM have been located in the magnetitite samples from the Nuasahi Massif. The assemblage is dominated by Pd-antimonides which account for 165 PGM making up over half of the PGM analyzed. A little over a quarter of the PGM, totaling 77, consist of Pd-Sb-oxides or Pd-Cu-oxides. Other Pd-bearing PGM in order of abundance include Pd-In, Pd-Pb alloys, Pd-sulfides, and minor occurrences of Pt-Pd alloy. Other Pt-bearing PGM include sperrylite ($PtAs_2$), the most abundant Pt-bearing PGM, and one grain of a Pt-Fe alloy. Rare Ru-, Rh-, Os-, and Ir-bearing PGM have been identified including laurite (RuS_2) and members of the irarsite-hollingworthite solid solution series (IrRhAsS), and both Rh and Ru are recorded in Co-Fe-sulpharsenides. Eight Au-bearing minerals accompany the PGM assemblage. The PGM have an average size of approximately 5 μm in diameter and the largest PGM is 33 × 12 μm. The variation in the numbers of the different PGM reveals the dominance of Pd-antimonides and their oxides (Fig. 6a). Calculated PGM abundance determined by the total area of each mineral type exposed on the surface of the polished block (Fig. 6b) shows that the Pd-antimonides and their oxides are even more dominant as they are larger than the other PGM. Quantitative analyses of the different PGM are shown in Table 2.

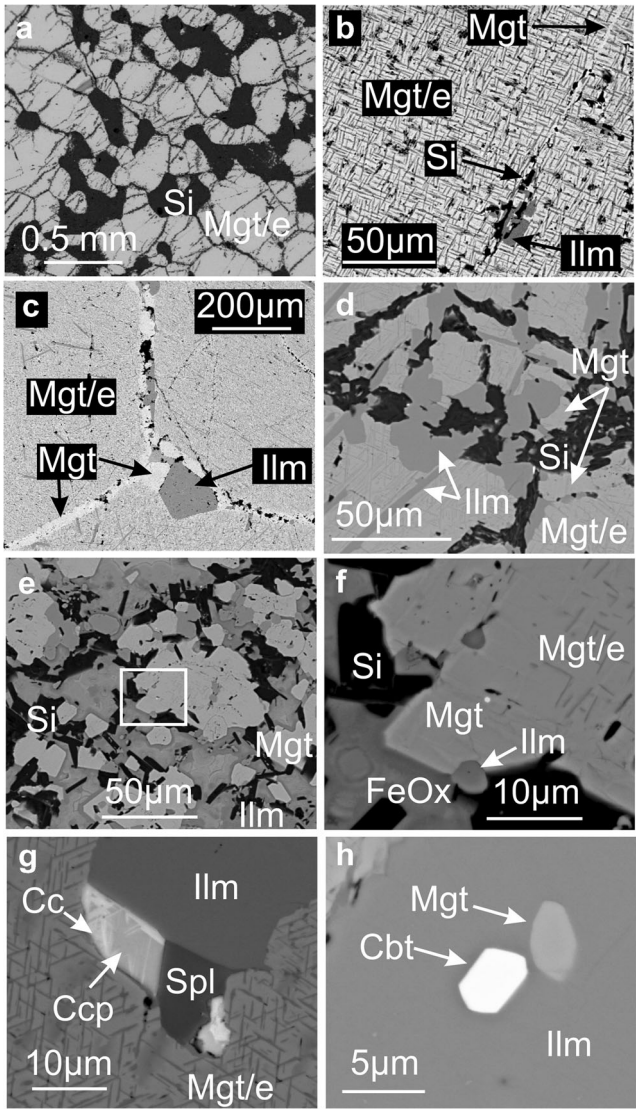

Fig. 4 Backscattered electron microscope images of magnetite textures. **a** Granular texture of magnetite (*Mgt/e*) (sample NSH/14/2). **b** Close up of a central magnetite grain showing the fine ilmenite exsolution texture that is characteristic of these magnetite grains. The image also shows a crosscutting vein similar to those that host PGM. The vein is filled with silicates (*Si*), ilmenite (*Ilm*), and magnetite (*Mgt*) (sample NSH/14/23). **c** Central magnetite grains with ilmenite and magnetite blebs along the grain boundaries, (sample NSH/14/5). **d** Typical texture at the edge of the central magnetite grains with blebs of ilmenite, magnetite, and silicate (sample NSH/14/13). **e** The central magnetite grains have been altered to blebs of ilmenite, magnetite, and silicate in this more extensively altered sample (sample NSH/14/13). **f** Close up of square area shown in **e** showing detail of ilmenite, magnetite, zoned iron oxides (FeOx), and silicates located around the central magnetite grains. **g** Chalcopyrite (*Ccp*) partially altered to chalcocite (*Cc*) associated with ilmenite and a Cr-bearing spinel (sample NSH/14/3). **h** Cobaltite (*Cbt*) and magnetite crystals in ilmenite (sample NSH/14/16)

The PGM occur commonly in clusters that are aligned in rows located in silicate- or ilmenite- or magnetite-filled veins that only crosscut the central magnetite grains. Platinum-group minerals enclosed within the central magnetite grains themselves, rather than in crosscutting rows, are very rare. Commonly, however, PGM are enclosed in ilmenite or magnetite blebs rimming the central magnetite grains. Platinum-group minerals are also common within interstitial silicates or at the junctions of ilmenite or magnetite blebs. Most of the PGM are isolated within the host oxides and silicates but occasionally composite PGM have been observed. Cu-sulfides are rare in these samples and only ten PGM are associated with Cu-sulfides. No Ni-bearing sulfides have been observed in association with the PGM.

Different PGM occur in different textural settings (Fig. 7), for example Pd-S, Pd-Pb, and Pd-In being confined to the central magnetite grains whereas the Pd-antimonides are more widespread but are predominantly associated with the magnetite and ilmenite blebs that surround the central magnetite grains. The PGM are described below in order of abundance and Fig. 8 includes the representative SEM images of the PGM, whereas the details are presented as ESM Fig. 8 (available online).

Pd-antimonides

There are two forms of Pd-antimonide. The most abundant is Pd_7Sb_3, which occurs in many textural associations, including in rows crosscutting central magnetite grains (Fig. 8a and ESM Fig. 8A), in blebs of magnetite and ilmenite surrounding central magnetite grains (ESM Fig. 8B), and in silicates and at the junctions of all these minerals. The Pd_7Sb_3 is usually subrounded, and when in interstitial silicates, it is frequently crossed by laths of chlorite and in some cases has an etched and corroded appearance (ESM Fig. 8C, D). It may take on a lath shape itself where it is surrounded by lath-shaped silicates. Commonly, Pd_7Sb_3 forms in clusters in interstitial silicates. This Pd-antimonide may contain a few wt% Te or Bi and in one case it contains Hg. One Pd-antimonide is enclosed by Cu-sulfides (Fig. 8b and ESM Fig. 8E).

The second Pd-antimonide is sudburyite (PdSb) that is only found enclosed in ilmenite grains surrounding the central magnetite grains (ESM Fig. 8F).

Pd-oxides

Commonly, Pd-antimonides are partially or completely altered to Pd-Sb-oxides especially when in contact with altered silicates. In samples that are poor in Pd-antimonides (e.g., samples NSH/14/23 and NSH/14/13), Pd-Cu-oxides are abundant and are also likely to be alteration products of more primary Pd-bearing PGM. The average size (5 × 3 μm) of the Pd-antimonides and the Pd-Sb-oxides is the same suggesting that the oxides have exactly pseudomorphed the more primary Pd-antimonides. The Pd-antimonides tend to have sharp straight crystal edges, whereas the oxides frequently have ragged outlines. All the Pd-oxides are characterized by intricate internal structures resulting in having a mottled appearance. This can either be delicate growths that form

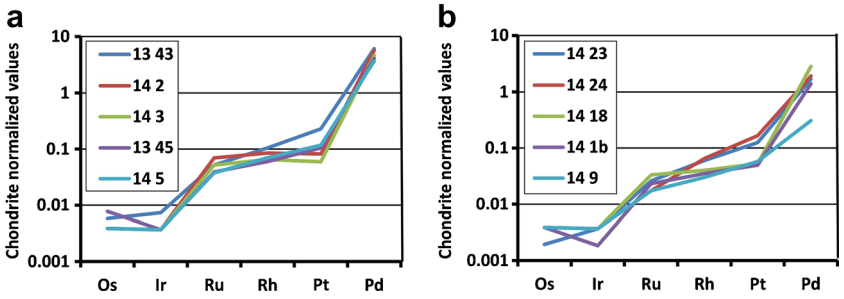

Fig. 5 Chondrite normalized PGE patterns for **a** the magnetitites with the highest PGE concentrations and **b** for magnetitites with lower PGE concentrations. Chondrite normalized values were taken from Naldrett and Duke (1980)

concentric rings (Fig. 8c, d and ESM Fig. 8G, H) or reticulate intergrowths of Pd-antimonide and Pd-oxide (ESM Fig. 8I, J). Sometimes, the Pd-antimonide is almost completely replaced internally by the Pd-Sb-oxide leaving a rim of Pd-antimonide around the edge of the composite PGM (ESM Fig. 8K). The internal areas show dendritic growth extending from the edge of the mineral and in two dimensions reveal cross sections of elongated fronds or of many circular cross sections of these fronds (ESM Fig. 8L). The coarseness of these Pd-oxide intergrowths varies (ESM Fig. 8M, N). Occasionally, the PGM appear to be breaking down as they oxidize with whiskers of PGM extending from them, suggesting local mobility and dispersion of the PGE (ESM Fig. 8O). The Pd-oxides vary in composition sometimes being Sb-rich and in other cases Cu-rich (ESM Fig. 8P).

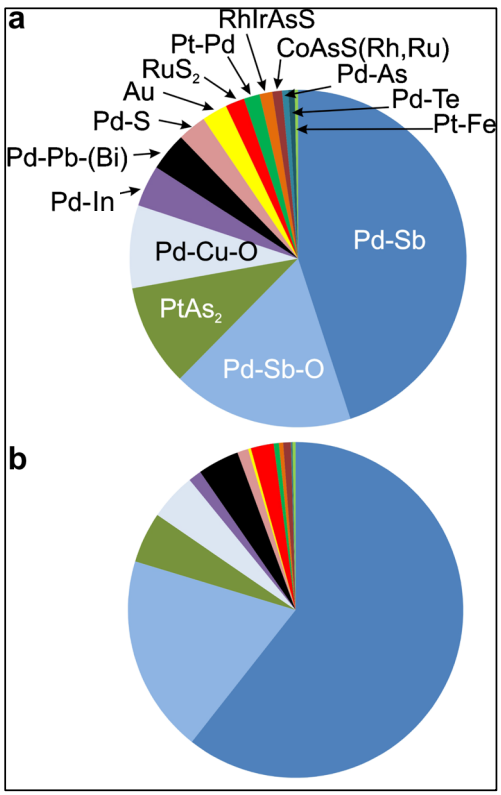

Fig. 6 Total abundance of PGM observed **a** by number of occurrences and **b** by area

Sperrylite

Sperrylite is the most common Pt-bearing PGM making up over 80% of the Pt-bearing PGM. It occurs in all textural sites including in rows across central magnetite grains and as composite grains with this Pd_7Sb_3 (ESM Fig. 8Q, R) but is mostly associated either within magnetite or ilmenite blebs or in interstitial silicate (Fig. 8e and ESM Fig. 8S–V). The sperrylite shows no alteration features. Its average size is only 2 × 3 μm.

Pd-sulfides

Pd-sulfides, mainly vysotskite, occur in two magnetitite samples. Their textural sites are much more restricted with most of them being in rows crosscutting central magnetite grains (Fig. 8f and ESM Fig. 8W) or rarely either enclosed within magnetite or on the edge of central magnetite grains (ESM Fig. 8X).

Pd-Pb

Pd-Pb alloys occur in only two magnetitite samples, and they are only present in rows that crosscut central magnetite grains

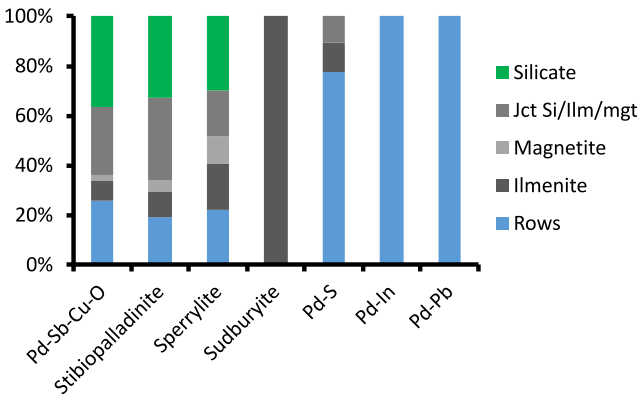

Fig. 7 Diagram illustrating the distribution of the major types of PGM located in different textural categories. The textural categories are within silicate (*Silicate*), at the contact of silicates and ilmenite blebs, magnetite blebs and central magnetite cores (*Jct Si/Ilm/mgt*), within magnetite blebs (*Magnetite*), and within ilmenite blebs (*Ilmenite*) around central magnetite grains and within rows crosscutting central magnetite grains (*Rows*). PGM are shown as a percentage of the total number of each type of PGM. Note that the numbers of different PGM are very variable: Pd-Sb-Cu-O = 77, Pd_7Sb_3 = 160, $PtAs_2$ = 37, PdSb = 5, Pd-S = 9, Pd-In = 13, and Pd-Pb = 10

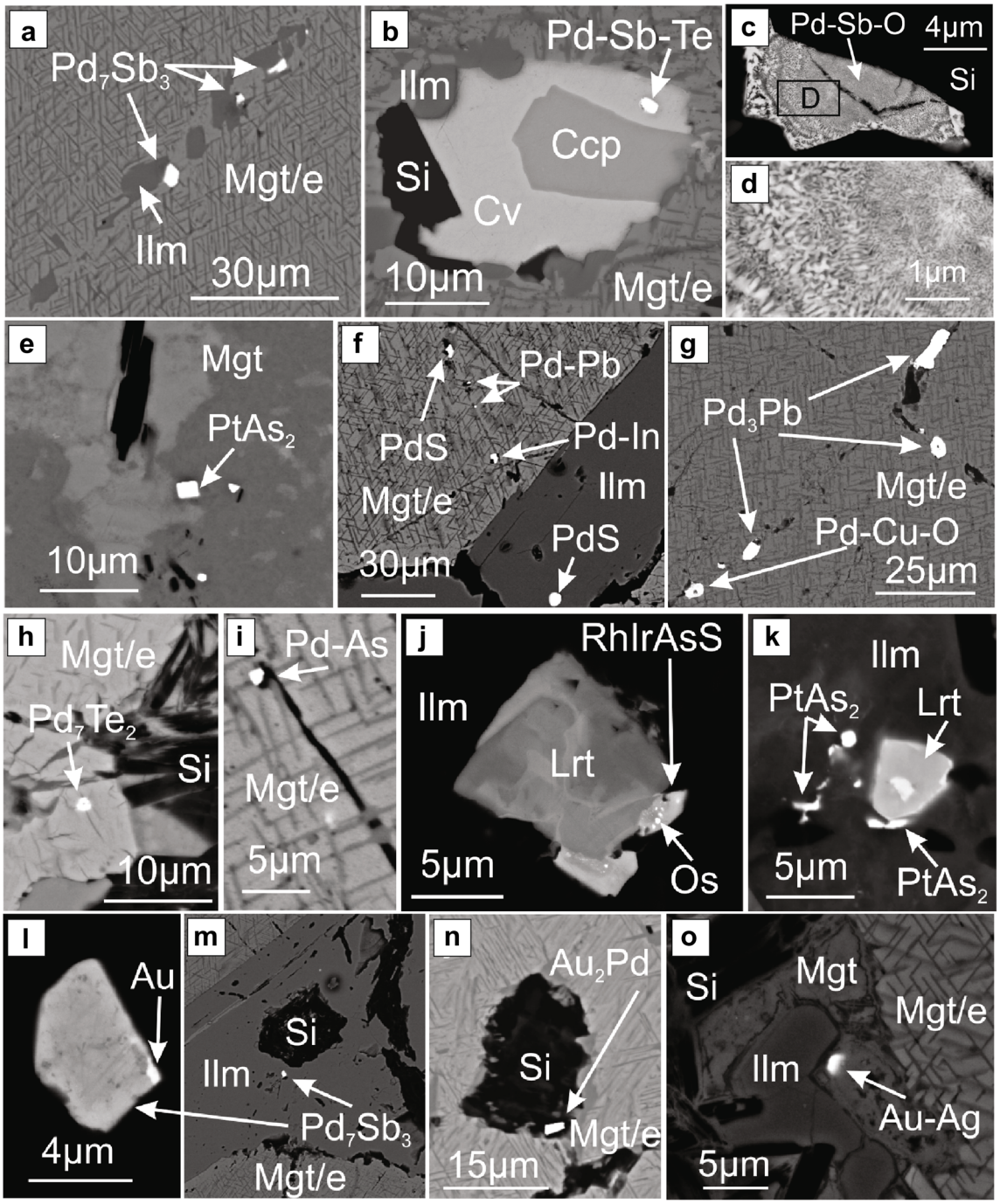

Fig. 8 Representative backscattered scanning electron (BSE) photomicrographs of the different varieties of PGM in the magnetitites showing textural positions of the PGM illustrated in order of abundance. Symbols used include *Mgt/e* central magnetite grain, *Mgt* magnetite, *Ilm* ilmenite and *Si* silicate, *Cv* chalcocite, *Ccp* chalcopyrite, and *Lrt* laurite. **a** Grains of stibiopalladinite in different textural settings in a row crosscutting a central magnetite grain (sample NSH/14/20). **b** Enclosed in chalcocite in a composite grain with chalcopyrite (sample NSH/13/45A). **c**, **d** Pd-oxides illustrating the textures of these minerals that are partially or completely altered Pd-antimonides. **c** A Pd-antimony oxide in silicate interstitial to magnetite (sample NSH/13/45A). **d** Close up of square area in **c** showing delicate intergrowths within the Pd-antimony oxide. **e** Euhedral grain of sperrylite in a magnetite bleb (sample NSH/14/3). **f** Pd-S, Pd-Pb, and Pd-ln are located in a row crosscutting a central magnetite grain with a Pd-S in ilmenite aligned with this row (sample NSH/14/23). **g** Zvyagintsevite and a Pd-Cu-oxide in rows crosscutting a central grain of magnetite, (sample NSH/13/43). **h** A Pd-telluride enclosed in magnetite (sample NSH/14/13). **i** A Pd-arsenide in a row crosscutting a central magnetite grain (sample NSH/14/23). **j** A composite grain of laurite and hollingworthite containing native osmium all enclosed in ilmenite, (sample NSH/13/45B). **k** A composite grain of laurite and sperrylite enclosed in ilmenite, (sample NSH/14/19). **l** Native Au on the edge of a stibiopalladinite grain (sample NSH/13/45A). **m** Location of **l** showing this composite grain enclosed in ilmenite. **n** Au-Pd in a silicate inclusion in a central magnetite grain (sample NSH/14/13). **o** Au-Ag grain in a bleb of magnetite (sample NSH/14/3)

(Fig. 8g and ESM Fig. 8Y) that also contain Pd-sulfides, Pd-In, Pd_7Sb_3, and Pd-Cu-oxides. Their composition suggests that they are zvyagintsevite (Pd_3Pb).

Rare Pd and Pt PGM

Pt-Pd alloys occur rarely, for example located at the edge of ilmenite adjacent to a silicate (ESM Fig. 8Z) and within silicates. One grain of Pd_7Te_2 occurs within but near the edge of a central magnetite grain (Fig. 8h and ESM Fig. 8a), and another occurs in a cluster of Pd_7Sb_3 in silicates. Three grains of Pd-As occur; one of which is located in a row of PGM that crosscuts a central magnetite grain (Fig. 8i and ESM Fig. 8b). One grain of Pt-Fe alloy has been observed in a cluster of fibrous magnetite surrounded by silicates (ESM Fig. 8c).

IPGM

Six laurites have been located in silicates (ESM Fig. 8d) or ilmenite blebs. They are euhedral in shape with rounded corners. The largest forms a composite grain with hollingworthite that contains blebs of native Os (Fig. 8j and ESM Fig. 8e). This particular laurite displays mottling due to a variable Os content. One laurite occurs with a cluster of sperrylite grains (Fig. 8k and ESM Fig. 8f). Hollingworthite is rare occurring with laurite enclosed in ilmenite and in silicates with Pd_7Sb_3 (Fig. 8j and ESM Fig. 8e, g).

Gold

Although Au-bearing grains are rare (eight grains) and small, averaging 1 μm in diameter, they have a very varied mineralogy composed of native Au, Au-Cu, Au-Pd, and Au-Ag. In one case, Au is concentrated on the edge of a Pd-antimonide all enclosed in ilmenite (Fig. 8l, m and ESM Fig. 8h, i). An Au_2Pd grain occurs within a silicate inclusion in a central magnetite grain (Fig. 8n and ESM Fig. 8j). The Au-Ag grains are enclosed in magnetite (Fig. 8o and ESM Fig. 8k) or silicates, and all other Au-bearing grains are enclosed in silicates.

PGE-bearing cobaltite

One or 2 wt% of Rh and Ru has been detected in different cobaltites in rare cases as shown, for example, in ESM Fig. 8m.

Pd-In

A possible new mineral to natural PGE ores has been observed in one sample and contains Pd and In. It occurs in rows that crosscut central magnetite grains. It is frequently present with several other PGM in these rows including Pd-Pb alloys and Pd-sulfides (Fig. 8f and ESM Fig. 8W). It forms 13 small grains that range from 1 × 1 to 5 × 5 μm and are too small for quantitative analysis but the presence of In is clear in the ED spectra (Fig. 9a, b) and qualitatively it has the composition Pd_3In or Pd_4In. Qualitative analyses also show that these Pd-In grains may contain up to 17 wt% Pb and Pb may be substituting for In.

Variation in the abundance of the different PGM between samples

Different magnetitite samples contain different assemblages of PGM (Fig. 10 and Table 3). For example, sample NSH/14/13, a massive coarse-grained magnetitite, is dominated by Pd-In, Pd-S, and Pd-Pb alloys that occur in rows crosscutting central magnetite, whereas sample NSH/13/45, a weathered magnetitite, contains more Pd-antimonides and Pd-oxides that are mainly located around the central magnetite grains with blebs of magnetite, ilmenite, and silicate. Some samples contain far fewer Pd-oxides, for example NSH/14/24, a massive sheared magnetitite, is dominated by unaltered Pd-antimonides and sperrylite, whereas NSH/14/18 is much more altered with Pd-Cu-oxides the most abundant PGM.

Discussion

A magmatic origin for the PGE mineralization

Evidence for an original primary magmatic origin of the PGE mineralization in the Nuasahi Massif comes from the lithological association of the PGE with the magnetitite. The

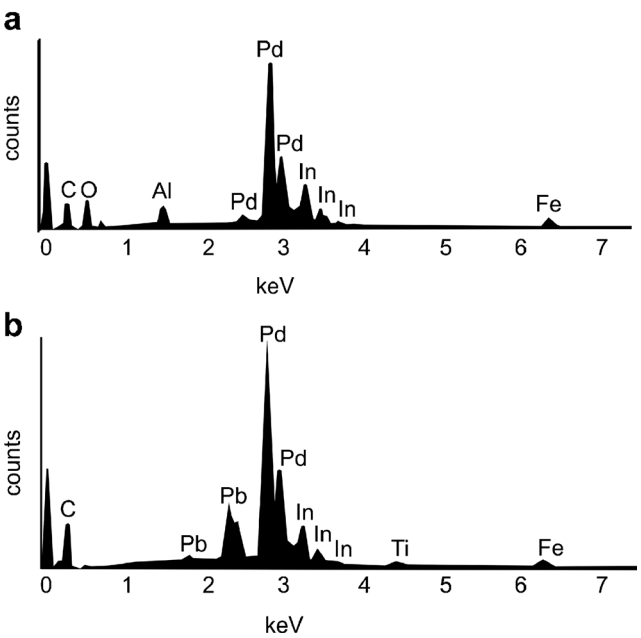

Fig. 9 Scanning electron microscope ED spectra showing the different compositions of In-bearing minerals suggesting a possible solid solution between In and Pb **a** Analysis of a Pd-In grain. **b** Analysis of a Pd-In-Pb grain

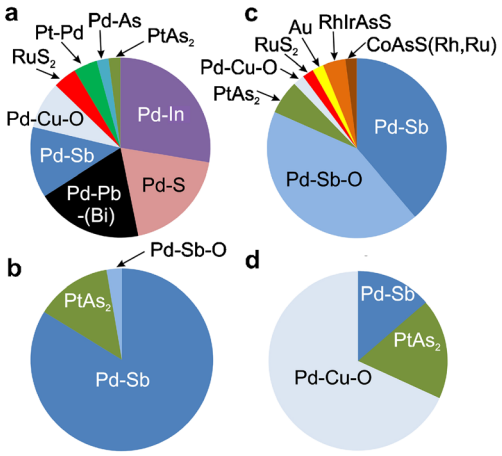

Fig. 10 Distribution of PGM in four magnetitite samples illustrating the different assemblages in each. **a** The most primary assemblage of PGM (sample NSH/14/23). [illustrated in Fig. 11a]. **b** A Pd-antimonide-dominated assemblage (sample NSH/13/24) [illustrated in Fig. 11b]. **c** A typical PGM assemblage (sample NSH/14/45). **d** An assemblage dominated by Pd-oxides (sample NSH/14/18) [illustrated in Fig. 11c]

distribution of the PGE in the magnetitite is clearly along the magnetitite layer rather than crosscutting it. This indicates a magmatic origin rather than a hydrothermal one where the mineralization is more likely to be in zones crosscutting the magmatic magnetitite layer.

Magmatic PGE concentrations associated with magnetite in the upper levels of layered complexes tend to be Pd- and Cu-bearing although Cu-sulfides are sparse, as for example in the Skaergaard Intrusion (e.g., Nielsen et al. 2015), the Freetown Intrusion (Bowles et al. 2013), and Rincón del Tigre (Prendergast 2000). It has been suggested that removal of FeO from magma during the crystallization of titanomagnetite causes sulfide saturation and this titanomagnetite re-equilibrates to magnetite and ilmenite on cooling (e.g., Haughton et al. 1974; Poulson and Ohmoto 1990; Prendergast 2000). Thus, an episode of sulfide saturation as the magnetitites formed causes crystallization of any remaining Cu-rich and Ni-poor fractionated sulfide liquid and PGE. The formation of the PGM in the magnetitites in the Nuasahi Massif may also be due to a magmatic sulfide saturation event that also was responsible for the formation of the Cu-sulfides, now represented by scarce chalcopyrite and its alteration minerals. The overall poor whole-rock base metal plus S and As concentrations in the magnetitites in the PGE-enriched magnetitite samples also support the above model (Table 1).

The Pd-rich (~3 ppm) and Pt-poor nature of the Nuasahi magnetitite is comparable to the Platinova Reef at Skaergaard (e.g., Andersen et al. 1998; Holwell and Keays 2014; Nielsen et al. 2015; Holwell et al. 2016). Both deposits have very low Ni and Cu. The Pd-rich and Pt-poor nature of the Platinova Reef at Skaergaard is due to late stage saturation in sulfide (and/or PGM), as discussed by Holwell et al. (2016), with Pt more compatible than Pd. This implies that the parental magma from which the magnetitites formed cannot have formed any of the PGE layers below, as that would have removed the Pd, and as such, this should give evidence of a new magma forming the upper gabbro unit with magnetitite in the Nuasahi Massif compared with the lower ultramafic unit. Previous studies by Mondal et al. (2001) and Khatun et al. (2014) showed that the lower ultramafic unit with chromitite ore bodies and the upper gabbro unit with magnetitites in the Nuasahi Massif were formed from two magmas: the lower ultramafic unit with chromitites was formed by fractional crystallization of a boninitic magma, whereas the upper gabbro with magnetitites was formed from mixed magmas that were produced by mixing of the residual evolved boninitic magma with batches of tholeiitic-like magmas. Late stage sulfide saturation of this magma produced the PGM in the magnetitites in the Nuasahi Massif.

Formation of the primary PGM

There is a clear sequence of formation for the different PGM in the Nuasahi magnetitite samples as revealed by different PGM assemblages occurring in different textural settings (Fig. 11). This is especially well illustrated by the Pd-bearing PGM.

The earliest PGM to form are Pd-Pb and Pd-In alloys that are entirely located in rows within the central magnetite grains (Fig. 8f, g and ESM Fig. 8W, Y). Pd-sulfides also belong to this early group of PGM as the vast majority of these also occur in these rows (Fig. 8f and ESM Fig. 8W, X). These rows and these PGM do not occur in the surrounding blebby magnetite and ilmenite and so are likely to have crystallized prior to the formation of this outer blebby zone. The rows that contain the PGM in the central magnetite may mark the positions of fractures that healed at high temperatures. The central magnetite grains exhibit an exsolution pattern that is absent in the surrounding blebby ilmenite and magnetite (e.g., Fig. 4b).

These primary Pd-In, Pd-Pb, and Pd-sulfides in the magnetitites differ from those described in the underlying breccia zone. However, a Pt-rich sulfide assemblage is described from the gabbro matrix of the breccias consisting of laurite, braggite, and malanite (Augé et al. 2002) and may be equivalent to the primary assemblage described here in these magnetitites.

The Pd_3In or Pd_4In alloys occurring in these central magnetite grains may be minerals new to natural rocks although these alloys are used in engineering (e.g., Okamoto 2003). In contrast, Pt-In is known from rocks as damiaoite $PtIn_2$ (Yu 1997a) and yixunite Pt_3In (Yu 1997b), both occurring in a Co-Cu-Pt-bearing vein in a garnet amphibole pyroxenite located near Damiao village on the Yixun River north of Beijing, China.

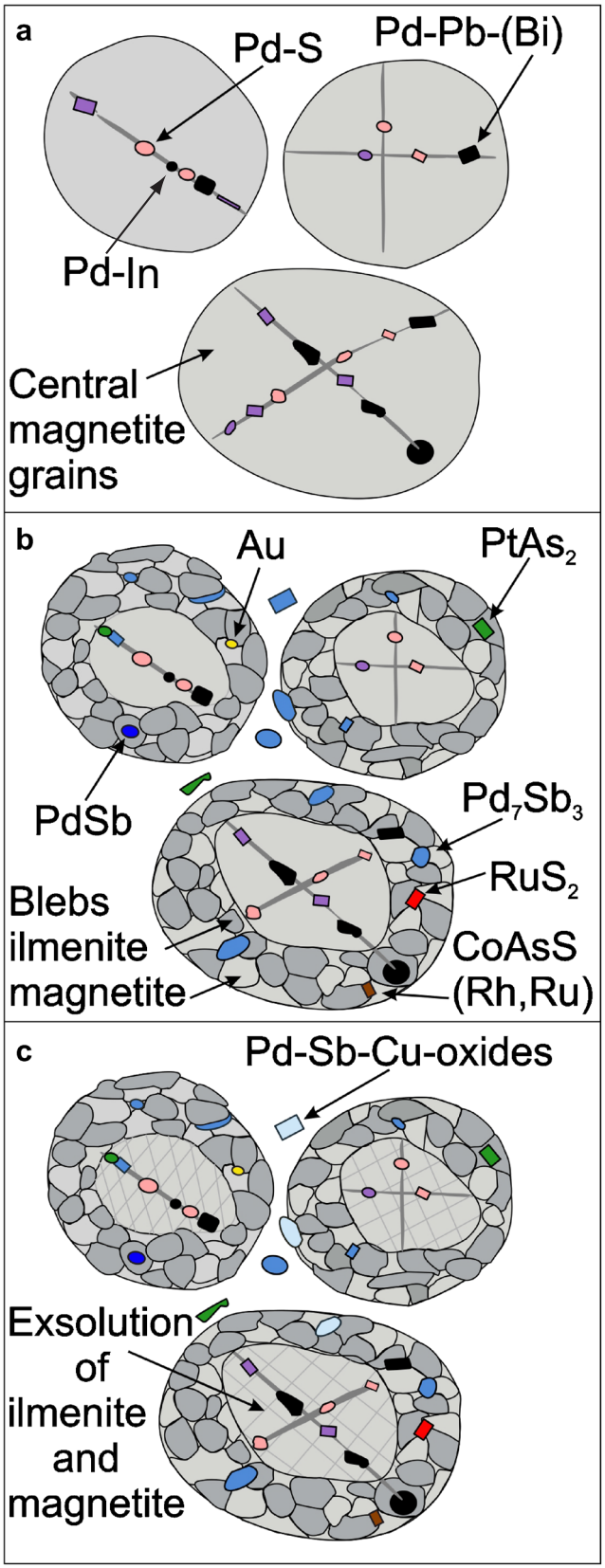

◀ **Fig. 11** Model illustrating the sequence of PGM formation. **a** Firstly, high temperature PGM Pd-S, Pd-Pb, and Pd-In form in rows in central magnetite gains. **b** Then, a later overprint producing the majority of the PGM, dominated by Pd-antimonides and accompanied by alteration of the rims of the central magnetite grains to blebs of ilmenite and magnetite. **c** Finally, complete cooling of magnetitite with the formation of the magnetite/ilmenite exsolution textures and weathering to produce Pd-oxides

Formation of Pd-antimonides, IPGM, and Au minerals

The blebby ilmenite and magnetite zones around the central magnetite are characterized by a second type of lower temperature exsolution termed granule-oxy-exsolution, where ilmenites migrate to magnetite grain boundaries forming blebs (Buddington and Lindsley 1964; Haggerty 1991; Fig. 4d, e). The Pd_7Sb_3 as well as the sperrylite are widely distributed occurring sometimes in rows that crosscut the central magnetites (Fig. 8a and ESM Fig. 8A, Q), but they are more abundant in the silicates (ESM Fig. 8C, D) or in the zone of ilmenite and magnetite blebs that surround the central magnetite grains (ESM Fig. 8B and Fig. 10). We propose that this is a second generation of PGM that has largely replaced the Pd-sulfides, Pd-Pb, and Pd-In alloys that are only present in the rows within the central magnetite grains. There also appears to be two generations of Pd-antimonides with an earlier PdSb situated entirely within ilmenite (ESM Fig. 8F) blebs that surround central magnetite grains and a later more widespread formation of Pd_7Sb_3 that rarely is enclosed by secondary Cu-sulfides (Fig. 8b and ESM Fig. 8E). Sperrylite (Fig. 8e and ESM Fig. 8Q–V), IPGM (Fig. 8e, f and ESM Fig. 8d–g), cobaltite (ESM Fig. 8m), and Au minerals (Fig. 8l–o and ESM Fig. 8h–k) are associated with the Pd-antimonides and belong to this later assemblage.

As in the magnetitites, the dominant and most widespread PGM assemblage described in the breccias are also dominated by Pd-antimonides (Mondal et al. 2001). So at both stratigraphic levels, an earlier PGE-sulfide assemblage has been modified by a later event that caused many of the more primary PGM to be altered to Pd-antimonides. Mondal et al. (2001) proposed that the alteration of the PGM sulfide assemblage to one dominated by antimonides in the breccias was due to a late magmatic hydrothermal event during the crystallization of the Nuasahi complex and so this secondary PGM assemblage in the magnetitites may have a similar late stage magmatic origin. Palladium antimonides can be found in mineral assemblages formed by early igneous crystallization but also may form during late stage hydrothermal environments (e.g., Mondal et al. 2001). Genesis of semi-metal-bearing PGM has been linked either to late magmatic fractionation of the PGE (Cabri and Laflamme 1976; Skinner et al. 1976) or to remobilization of the PGE during a later hydrothermal stage (e.g., Ballhaus and Stumpfl 1986). Previous O and H isotope studies of low-temperature assemblages of the breccia

zone and the serpentinite from the lower ultramafic unit and the altered assemblages of the upper gabbro unit showed that the entire igneous complex including the breccia assemblages had interacted with evolved seawater at a later stage (Mondal et al. 2002, 2003; Mondal 2009). However, an S isotope study indicates that mantle-derived sulfides formed the BMS and PGE-rich assemblages in the breccia zone (Mondal et al. 2002; Mondal 2009). Recent research based on the pattern of fluid-mobile element mobilization (e.g., Li and B) during replacement suggests that the serpentinization of the Nuasahi dunite and harzburgite occurred during interaction with a B-rich solution, possibly in an ocean-floor setting (Majumdar et al. 2016a, b). It is unclear in the Nuasahi Massif when the alteration of the PGM to antimonides took place.

The presence of the Pd-antimonides and sperrylite requires the presence of the semi-metals As and Sb for their formation. Sperrylite has been described as a high temperature magmatic mineral crystallizing before sulfur saturation, for example, in the Sudbury Igneous complex (Dare et al. 2010). In other complexes (e.g., Shetland ophiolite complex), the As is clearly late having been introduced by a hydrothermal event that occurred after the formation of the igneous complex. In the Shetland ophiolite complex, the highest PGE concentrations are associated with Cu-sulfides in wehrlites. In this occurrence, the Cu-bearing primary assemblage within fresh clinopyroxene contains Pd-Cu-sulfide and Pd-Pb alloy. This PGE-assemblage was overprinted post-emplacement of the ophiolite by Sb, Te, and As that altered the PGM to antimonides, tellurides, and arsenides (Prichard et al. 1994).

In the Freetown and Skaergaard Intrusions, the PGE are at high levels associated with magnetitite layers but actually occur in the surrounding gabbros and anorthosites (Bowles et al. 2013; Nielsen et al. 2015) as is the case for the Bushveld Complex where the PGE are located in anorthosites just below the magnetitites (Harney et al. 1990). The Nuasahi Massif PGE occurrence in the high-level magnetitites is most like those in the Stella intrusion (Maier et al. 2003) and in the Rio Jacaré Sill (Sá et al. 2005), because in all three occurrences the PGE are concentrated within the high-level magnetitites themselves. The PGM in the Stella complex are mostly sperrylite (Maier personal communication). So the PGM in the Nuasahi Massif are most likely those in the Rio Jacaré Sill which are dominated by Pd-Sb-Bi-tellurides and sperrylite with minor Pt-antimonides, Pd-Ni arsenides, hollingworthite, Pd-Cu-Sn alloys, Au-Cu-Pd, Pt-Cu, Pt-Au, Pt-Fe, and Pt-Ni (Sá et al. 2005). In the Rio Jacaré Sill, the Pd-antimonides are enclosed in magnetite or ilmenite blebs in close association with silicate and spinel inclusions and the assemblage probably has been recrystallized completely to an assemblage similar to the magnetite and ilmenite blebs that surround the central magnetite grains present in the Nuasahi magnititites. The central magnetite grains present in the Nuasahi magnetitites have not been observed in the Jacaré Sill. Similar to the Nuasahi magnetitites, the Pd-bearing PGM in the Rio Jacaré Sill magnetitites are typically associated with magnetite, ilmenite, or at the grain boundaries between magnetite and ilmenite or silicate. Other similarities include the presence of Pd-Pb alloys enclosed in magnetite and the presence of sperrylite more commonly in the silicates than in the magnetite- or ilmenite-rich parts of the magnetitite in Rio Jacaré Sill.

Formation of the Pd-oxides

Lastly, the Pd-antimonides in the magnetitites are frequently replaced either by Pd-Sb-oxides or Pd-Cu-oxides (Fig. 8c and d and ESM Fig. 8G–P). It is likely that these formed during tropical weathering of the magnetite. Some of the first Pt-Fe oxides were described from ophiolites in New Caledonia (Augé and Legendre 1994) and from the Shetland ophiolite (Prichard et al. 1994). In the Main Sulfide Zone of the Great Dyke of Zimbabwe, it was observed that some PGM are more prone to oxidation than others, so Pt-Pd-Bi-tellurides and sulfarsenides are replaced by PGE-oxides whereas sperrylite, cooperate, braggite, and laurite tend to remain unaltered (Oberthür et al. 2003). The resistance of sperrylite to alteration was also observed in the Aguablanca gossan where the Pd-bearing PGM are readily oxidized to Pd-Cu-oxides and hydroxides, and these frequently have ragged edges and appear to be disintegrating (Suárez et al. 2010). In this case, the Pd as well as the other PGE are dispersed from the PGM into the surrounding Fe oxides (Suárez et al. 2010). The resistance of sperrylite to alteration in the Nuasahi Massif magnetitites is also clear compared with the Pd-bearing PGM. The extreme dispersal and disintegration of the Pd-oxides do not appear to have occurred in these magnetitites with the Pd-oxides forming pseudomorphs of the earlier more primary Pd-bearing PGM. Oxidation of PGM usually occurs during weathering of the PGE-rich lithologies (Oberthür et al. 2003; Suárez et al. 2010), and this may also be the case for the magnetitites that have been subjected to weathering in the hot and wet Indian climate.

Vanadium in the magnetitites

It is interesting to note that in the Nuasahi magnetitites vanadium values are low, with a maximum of 0.5 wt% V_2O_5 in the magnetite grains in a two of the magnetitites analyzed. The underlying gabbro in the Nuasahi Massif formed from the same magma from which the parental magma of the magnetitite layers was evolved (Khatun et al. 2014). Clinopyroxene is known to remove V from magma during crystallization and the partition of V into magnetite is also

critically dependent on the oxygen fugacity of the magma (Toplis and Corgne 2002). Therefore, the parental magma was probably V-depleted during formation of the magnetitite layers as the clinopyroxene in the underlying gabbro might have removed the V. In contrast to the low values in the Nuasahi magnetitites, the V_2O_5 in the Rio Jacaré Sill for example ranges from 0.3 to 4.5 wt% (Brito 2000) with an average of 1.3 wt% (Galvão et al. 1986) and in Rincón del Tigre ranges up to over 1 wt% (Prendergast 2000).

Economic significance of the Pd in the Nuasahi magnetitites

Small bodies with anomalous ppm Pd concentrations of only the order of 1–2 km can be economic as demonstrated by the Lac des Iles deposit in Canada where the deposit occurs in the upper part of the complex in breccias. In Lac des Iles, the measured and indicated resources of the Pd deposits are 32.2 million tons at 3.28 g/t Pd and 0.26 g/t Pt (Djon and Barnes 2012). The oldest and most economically significant PGE mineralization within gabbro-hosted magnetitites has been reported from the 3.0-Ga Stella intrusion in the Kraipaan Greenstone Belt (Republic of South Africa) where Pt and Pd occur in reefs (Pt+Pd ~15 ppm; Maier et al. 2003). The present study shows that in the Nuasahi Massif the magnetitite layer within the upper gabbro has a ~1-km-long zone parallel to the strike of the layering and an average thickness of 9 m. It contains consistent total PGE concentrations of part per million values up to 3.6 ppm. The 17 samples collected from the kilometer-long PGE zone have an average PGE concentration of 1685 ppb (~1.7 ppm). As continuation of the PGE concentrations in the magnetitites has been located at the southern end of the magnetite layer, there is a significant possibility of expanding the potential of the PGE zone.

Conclusions

This example of Pd and Cu concentrations in the Nuasahi magnetitites is similar to other Pd- and Cu-rich occurrences located in the upper parts of layered intrusions. These are thought to form as a result of a late sulfide saturation event from an evolved sulfide and PGE-bearing silicate magma during crystallization of magnetitites. Widespread distribution of Pd anomalies of more than 1 ppm within the Nuasahi Massif magnetitite layer rather than in crosscutting zones also indicates a lithologic control to the mineralization, indicating a magmatic rather than a hydrothermal origin for the mineralization.

The PGM show a sequence of formation with initial Pd-sulfides, Pd-Pb, and Pd-In alloys forming in rows that only crosscut central magnetite grains in the magnetitites. Subsequent magmatic hydrothermal overprinting of the magnetitites caused the replacement of the primary assemblage to form abundant Pd-antimonides that may have crystallized at the same time as those associated with the underlying PGE- and BMS-rich gabbro breccia. Finally, many of the PGM were oxidized probably during weathering in the hot and wet climate of this part of India. These PGE concentrations in the magnetitites may be of interest for further study to demonstrate possible economic potential. This discovery suggests that "conduit type" complexes with thick chromitites are prospective for PGE not only in gabbro breccias but also in any overlying magnetitites.

Acknowledgments Research carried out was part of a UGC-UKIERI Thematic Partnership project 2013-003 (F-184-1/2013-IC) entitled "Sustainable resourcing of platinum-group elements (PGE): studies to understand and locate PGE in chromitities and breccias in India" (project website: iptri.in). Mining authorities OMC and IMFA are acknowledged for their support during fieldwork. John Bowles and Dave Holwell, the official reviewers of the journal, are acknowledged for the constructive review of the article. We are thankful to Bernd Lehmann (Editor-in-Chief of the journal) and Marco Fiorentini (Associate Editor of the journal) for useful editorial comments on this article.

References

Alapieti TT, Kujanpaa J, Lahtinen JJ, Papunen H (1989) The Kemi stratiform chromitite deposit northern Finland. Econ Geol 84:1057–1077

Andersen JCØ, Rasmussen H, Nielsen TFD, Ronsbo JC (1998) The Triple Group and the Plat nova gold and palladium reefs in the Skaergaard intrusion: stratigraphic and petrographic relations. Econ Geol 93:488–509

Augé T, Legendre O (1994) Platinum-group element oxides from the Pirogues ophiolitic mineralization, New Caledonia: origin and significance. Econ Geol 89:1454–1468

Augé T, Salpeteur I, Bailly L, Mukherjee MM, Patra RN (2002) Magmatic and hydrothermal platinum-group minerals and base-metal sulfides in the Baula Complex. India Can Mineral 40:277–309

Augé T, Cocherie A, Genna A, Amstrong R, Guerrot C, Mukherjee MM, Patra RN (2003) Age of the Baula PGE mineralization (Orissa, India) and its implications concerning the Singhbhum Archean Nucleus. Precambrian Res 121:85–101

Ballhaus CG, Stumpfl EF (1986) Sulfide and platinum mineralization in the Merensky Reef: evidence from hydrous silicates and fluid inclusions. Contrib Mineral Petrol 94(2):193–204

Barnes S-J, Maier WD, Ashwal LD (2004) Platinum-group element distribution in the Main Zone and Upper Zone of the Bushveld Complex, South Africa. Chem Geol 208:294–317

Barnes S-J, Pagé P, Prichard HM, Zientek ML, Fisher PC (2015) Chalcophile and platinum-group element distribution in the Ultramafic series of the Stillwater Complex, MT, USA—implications for processes enriching chromite layers in Os, Ir, Ru, and Rh. Mineral Deposita 51:25–47

Bowles JFW, Prichard HM, Suárez S, Fisher PC (2013) The first report of platinum-group minerals in magnetite-bearing gabbro, Freetown Layered Complex, Sierra Leone: occurrences and genesis. Can Mineral 51:455–473

Brito RSC (2000) Geologia e petrologia do sill máfico ultramáfico do Rio Jacaré, Bahia e estudo das mineralizações de Fe-Ti-V e platinóides

asociados. Unpublished Ph D. thesis, Brasilia, Brazil, Universidade de Brasília, no 39, 325

Buddington AF, Lindsley DH (1964) Iron–titanium oxide minerals and synthetic equivalents. J Petrol 5:310–357

Cabri LJ, Laflamme JHG (1976) The mineralogy of the platinum-group elements from some copper-nickel deposits of the Sudbury area, Ontario. Econ Geol 71(7):1159–1195

Carson HJE, Lesher CM, Houlé MG, Weston RJ, Metsaranta RT, Shinkle DA (2013) Komatiite-associated Cr and Ni-Cu-PGE mineralization in the Black Tor–Black Label Ultramafic intrusive complex, McFaulds Lake Greenstone Belt. In: Mineral Deposit research for a high-tech world, 12th BIennial SGA Meeting, Uppsala, p 960-963

Chakraborty KL (1959) Mineragraphic study of the vanadium-bearing titaniferous magnetites associated with the gabbro-anorthosites of Nuasahi, Keonjhar district, Orissa, India—their textural relations and paragenesis. Proc Nat Inst Sci India 25A:262–272

Chakraborty KL, Roy J, Majumder T (1988) Structures and textures of vanadium bearing titaniferous magnetite ores and their interpretation. J Geol Soc India 31:305–313

Dare SAS, Barnes S-J, Prichard HM (2010) The distribution of platinum-group elements (PGE) and other chalcophile elements among sulfides from Creighton Ni-Cu-PGE sulfide deposit, Sudbury, Canada, and the origin of palladium in pentlandite. Mineral Deposita 45: 765–793

Djon MLN, Barnes S-J (2012) Changes in sulfides and platinum-group minerals with the degree of alteration in the Roby, Twilight, and High Grade Zones of the Lac des Iles Complex, Ontario, Canada. Mineral Deposita 47:875–896

Galvão CF, Vianna IA, Nonato IFBP, Brito RSC (1986) Depósito de magnetita vanadífera da fazenda Gulçari, Maracás, Bahia. In Schobbenhaus C, Coelho CES (ed) Principais depósitos minerais do Brasil. National Department of Mineral Production (DNPM), Brasília, vol 2 (XL), p 493-501

Ghosh AMN, Prasada Rao GHSV (1952) Some observations on the chromite occurrences of Nuasahi, Keonjhar district, Orissa. Geol Survey India Rec 82:281–299

Haggerty SE (1991) Oxide textures—a mini-atlas. In: Lindsley DH, Ribbe PH (eds) Oxide minerals: petrologic and magnetic significance, Reviews in mineralogy, vol, vol 25, pp 129–219

Haldar D, Chatterjee PK (1976) Interrelationship of the ultramafic and mafic granophyric suites of rocks in the Nausahi-Nilgiri Belt, Orissa. Misc Publ Geol Survey India 23(part 2):299–309

Harney DMW, Merkle RKW, Von Gruenewaldt G (1990) Platinum-group element behavior in the lower part of the upper zone, eastern Bushveld Complex: implications for the formation of the main magnetite layer. Econ Geol 85:1777–1789

Hauck SA, Severson MJ, Zanko L, Barnes S-J, Morton P, Alminas H, Foord EE, Dahlberg EH (1997) An overview of the geology and oxide, sulfide, and platinum-group element mineralization along the western and northern contacts of the Duluth Complex. In: Ojiakangas RW, Dickas AB, Green JC (ed) Middle Proterozoic to Cambrian Rifting, Central North America. Geol Soc Am Spec Paper 312, p 137–187

Haughton DR, Roeder PL, Skinner BJ (1974) Solubility of sulfur in mafic magmas. Econ Geol 69:451–467

Holwell DA, Keays RR (2014) The formation of low volume, high tenor magmatic PGE-Au sulphide mineralisation in closed systems: evidence from precious and base metal geochemistry of the Platinova Reef, Skaergaard Intrusion, East Greenland. Econ Geol 109:387–406

Holwell DA, Barnes SJ, Margaux LV, Keays RR, Fisher LA, Prasser R (2016) 3D textural evidence for the formation of ultra-high tenor precious metal bearing sulphide microdroplets in offset reefs: an extreme example from the Platinova Reef, Skaergaard Intrusion, Greenland. Lithos 256–257:55–74

Khatun S, Mondal SK, Zhou MF, Balaram V, Prichard HM (2014) Platinum-group element (PGE) geochemistry of Mesoarchean ultramafic–mafic cumulate rocks and chromitites from the Nuasahi Massif, Singhbhum Craton (India). Lithos 205:322–340

Leelananadam C, Burke K, Ashwal LD, Webb SJ (2006) Proterozoic mountain building in Peninsular India: an analysis based primarily on alkaline rock distribution. Geol Mag 143:1–18

Lesher CM, Carson HJE, Metsaranta RT, Houlé MG (2014) Genesis of chromite deposits by partial melting, physical transport, and dynamic upgrading of silicate-magnetite facies iron formation. 12th IPS Ekaterinburg, Russia, Abstract 59

Lord RA, Prichard HM, Sá JHS, Neary CR (2004) Chromite geochemistry and PGE fractionation in the Campo Formoso and Ipueira-Medrado Sill, Bahia State, Brazil. Econ Geol 99:339–363

Maier WD, Barnes S-J, Gartz V, Andrews G (2003) Pt-Pd reefs in magnetitites of the Stella layered intrusion, South Africa: a world of new exploration opportunities for platinum-group elements. Geology 31:885–888

Majumdar AS, Hövelmann J, Vollmer C, Berndt J, Mondal SK, Putnis A (2016a) Formation of Mg-rich olivine pseudomorphs in serpentinized dunite from the Mesoarchean Nuasahi Massif, eastern India: insights into the evolution of fluid composition at the mineral-fluid interface. J Petrol 57:3–26

Majumdar AS, Hövelmann J, Mondal SK, Putnis A (2016b) The role of reacting solution and temperature on compositional evolution during harzburgite alteration: constraints from the Mesoarchean Nuasahi Massif (eastern India). Lithos 256–257:228–242

Melcher F, Grum W, Simon G, Thalhammer TV, Stumpfl EF (1997) Petrogenesis of the ophiolitic giant chromite deposits of Kempirsai, Kazakhstan: a study of solid and fluid inclusions in chromite. J Petrol 38:1419–1458

Mohanty JK, Paul AK (2008) Fe-Ti-oxide ore of the Mesoarchean Nuasahi Ultramafic-Mafic Complex, Orissa and its utilization potential. J Geol Soc India 72:623–633

Mondal SK (2000) Study of chromite, sulfide and noble metal mineralization in the Precambrian Nuasahi ultramafic–mafic complex, Keonjhar district, Orissa, India. Unpublished Ph D. thesis. Jadavpur University. Calcutta, India, 193 p

Mondal SK (2009) Chromite and PGE deposits of Mesoarchaean ultramafic-mafic suites within the greenstone belts of the Singhbhum craton, India: implications for mantle heterogeneity and tectonic setting. J Geol Soc India 73:36–51

Mondal SK, Baidya TK (1997) Platinum-group minerals from the Nuasahi ultramafic-mafic complex, Orissa, India. Min Mag 61: 902–906

Mondal SK, Mathez EA (2007) Origin of the UG2 chromitite layer, Bushveld Complex. J Petrol 48:495–510

Mondal SK, Prichard HM (2016) PGE-rich chromitite bands in the Mesoarchean Nuasahi and Sukinda Massifs, Singhbhum Craton (India). GOLDSCHMIDT 2016-Yokohama (Japan), abstract no 2130

Mondal SK, Zhou M-F (2010) Enrichment of PGE through interaction of evolved boninitic magmas with early formed cumulates in a gabbro–breccia zone of the Mesoarchean Nuasahi Massif (eastern India). Mineral Deposita 45:69–91

Mondal SK, Baidya TK, Rao KNG, Glascock MD (2001) PGE and Ag mineralization in a breccia zone of the Precambrian Nuasahi ultramafic-mafic complex, Orissa, India. Can Mineral 39:979–996

Mondal SK, Ripley EM, Li C, Mariga J (2002) Stable isotopic studies of the chromite, Fe-Cu-Ni-sulfide and PGE mineralized Archean Nuasahi ultramafic-mafic complex, Orissa, India. Geol Soc America Annual Meeting, Denver, Paper no 52–4

Mondal SK, Ripley EM, Li C, Ahmed AH, Arai S, Liipo J, Stowe C (2003) Oxygen isotopic compositions of Cr spinels from Archaean to Phanerozoic chromite deposits. Geochim Cosmochim Acta Suppl 67(18):301

Mondal SK, Ripley EM, Li C, Frei R (2006) The genesis of Archean chromitites from the Nuasahi and Sukinda massifs in the Singhbhum craton, India. Precambrian Res 148:45–66

Mukherjee R, Mondal SK, Frei R, Rosing MT, Waight TE, Zhong H, Kumar GRR (2012) The 3.1 Ga Nuggihalli chromite deposits, Western Dharwar craton (India): geochemical and isotopic constraints on mantle sources, crustal evolution and implications for supercontinent formation and ore mineralization. Lithos 155:392–409

Mungall JE (2014) Geochemistry of magmatic ore deposits. Treatise on geochemistry, 2nd Edition, vol 13, p 195–218

Naldrett AJ, Duke JM (1980) Platinum metals in magmatic sulfide ores. Science 208:1417–1428

Naldrett AJ, Kinnaird JA, Wilson A, Yudovskaya MA, McQuade S, Chunnett G, Stanley C (2009) Chromite composition and PGE content of Bushveld chromitites: part 1. The lower and middle groups. Trans Inst Min Metall 118:131–161

Nielsen TFD, Andersen JCØ, Holness MB, Keiding JK, Rudashevsky NS, Rudashevsky VN, Salmonsen LP, Tegner C, Veksler IV (2015) The Skaergaard PGE and gold deposit: the result of in situ fractionation, sulfide saturation, and magma chamber-scale precious metal redistribution by immiscible Fe-rich melt. J Petrol 56:1643–1676

Oberthür T, Weiser TW, Gast L (2003) Geochemistry and mineralogy of platinum-group elements at Hartley Platinum Mine Zimbabwe. Part 2: supergene redistribution in the oxidized Main Sulfide Zone of the Great Dyke, and alluvial platinum-group minerals. Mineral Deposita 38:344–355

Okamoto H (2003) In-Pd (indium-palladium). J Phase Equilibria 24:481–481

Poulson SR, Ohmoto H (1990) An evaluation of the solubility of sulfide sulfur in silicate melts from experimental data and natural samples. Chem Geol 85:57–75

Prendergast MD (2000) Layering and precious metals mineralization in the Rincón del Tigre Complex, Eastern Bolivia. Econ Geol 95:113–130

Prendergast MD (2008) Archean komatiitic sill-hosted chromite deposits in the Zimbabwe Craton. Econ Geol 103:981–1004

Prichard HM, Ixer RA, Lord RA, Maynard J, Williams N (1994) Assemblages of platinum-group minerals and sulfides in silicate lithologies and chromite-rich rocks within the Shetland ophiolite. Can Mineral 32:271–294

Prichard HM, Sá JHS, Fisher PC (2001) Platinum-group mineral assemblages and chromite composition in the altered and deformed Bacuri complex, Amapa, Northeastern Brazil. Can Mineral 39:377–396

Radhakrishna BP, Naqvi SM (1986) Precambrian continental crust of India and its evolution. J Geol 94:145–166

Sá JHS, Prichard HM, Barnes S-J, Fisher PC (2005) The distribution of base metals and platinum-group elements in magnetitite and its host rocks in the Rio Jacaré Intrusion, Northeastern Brazil. Econ Geol 100:333–348

Saha AK (1994) Crustal evolution of Singhbhum North Orissa. Eastern India Geol Soc India Memoir 27:341 p

Sarkar SC (1959) Origin of the titaniferous and vanadium-bearing magnetite ores of Nuasahi, Keonjhar, Orissa. Sci Cult 24:383–384

Sengupta S, Acharya SK, De Smeth JB (1997) Geochemistry of Archaean volcanic rocks from Iron Ore supergroup, Singhbhum, eastern India. Proc Indian Acad Sci (Earth Planetary Sciences) 106:327–342

Skinner BJ, Luce FD, Dill JA, Ellis DE, Hagan HA, Lewis DM, Odell DA, Sverjensky DA, Williams N (1976) Phase relations in ternary portions of the system Pt-Pd-Fe-As-S. Econ Geol 71(7):1469–1475

Stowe CW (1994) Compositions and tectonic settings of chromite deposits though time. Econ Geol 89:528–546

Suárez S, Prichard HM, Velasco F, Fisher PC, McDonald I (2010) Alteration of platinum-group minerals and dispersion of platinum-group elements during progressive weathering of the Aguablanca Ni-Cu deposit, SW Spain. Mineral Deposita 45:331–350

Toplis MJ, Corgne A (2002) An experimental study of element partitioning between magnetite, clinopyroxene and iron-bearing liquids with particular emphasis on vanadium. Contrib Mineral Petrol 144:22–37

Varma OP (1964) The geology and origin of magnetite deposits of the Baula Range near the village of Nausahi District, Keonjhar, (Orissa). Quart J Geol Min Met Soc India 36:1–12

Varma OP (1986) Some aspects of ultramafic and ultrabasic rocks and related chromite metallogenesis with examples from eastern region of India. Indian Science Congress Association, Proceedings of the 73rd session, part 2, p 1–72

Yu Z (1997a) Damiaoite—a new native indium and platinum alloy. Acta Geol Sin 71:336–339

Yu Z (1997b) Yixunite—an ordered new native indium and platinum alloy. Acta Geol Sin 71:333–335